Supplementary Information

Co-existence of Five- and Six-Coordinate Iron(II) Species Captured in a Geometrically Strained Spin-Crossover Hofmann Framework

Luonan Xu,[a] Zixi Xie,[b] Katrina A. Zenere,[b] Jack K. Clegg,[c] Elise Kenny,[d] Nicole J. Rijs,[a] Guy N. L. Jameson,[e] Cameron J. Kepert,*[b] Benjamin J. Powell*[d] and Suzanne M. Neville*[a]

[a]School of Chemistry, The University of New South Wales, Sydney, New South Wales, 2052, Australia.

[b]School of Chemistry, The University of Sydney, Sydney, New South Wales, 2006, Australia.

[c]School of Chemistry and Molecular Biosciences, The University of Queensland, St Lucia, Queensland, 4072, Australia.

[d]School of School of Mathematics and Physics, The University of Queensland, St Lucia 4072, Queensland, Australia.

[e]School of Chemistry, Bio21 Molecular Science and Biotechnology Institute, The University of Melbourne, 30 Flemington Road, Parkville, Victoria 3010, Australia.

CONTENTS

1.   Experiment methods

Single crystal X-ray diffraction. Single crystal X-ray diffraction data were collected on a Bruker D8 QUEST or Rigaku Synergy diffractometer operating with Mo-Kα (λ = 0.71073 Å) radiation. Data were collected at 10 K intervals over the range 250 to 100 K. The crystals were mounted on a cryoloop in paratone oil. Data collection, integration, reduction and absorption corrections were performed using either the APEX3 software package or CrysalisPro.[1-2] Strucures were solved using SHELXT-2018 by direct methods and refined with SHELXL-2014 in OLEX2.[3-4] Structual refinement details are presented in Table S2 and selected structural parameters are presented in Table S3. A representative asymmetric unit is shown in Figure S4 (250 and 100 K). The crystallographic data in CIF format were deposited at the Cambridge Crystallographic Data Centre with CCDC Nos. 2162711-2162712.

Powder diffraction using synchrotron radiation. Variable temperature X-ray powder diffraction data were collected on the Powder Diffraction beamline (BL-10; 21.00 keV and 0.5895 Å) at the Australian Synchrotron.[5] A freshly prepared polycrystalline sample of 1 was gently ground into a slurry with a small amount of mother liquor with care to avoid any solvent loss and then packed into glass capillary tube (0.5 mm diameter) with some mother liquor retained to ensure the sample was completely solvated; the capillary was fused shut to avoid any solvent loss during measurement. The capillary was rotated at ca. 1 Hz during data collection to aide powder averaging. The wavelength was determined accurately using NIST SRM LaB6 660b standard. Temperature-dependent data were collected upon cooling and warming in steps of 120 K h^{-1} from 250-120-250 K. Data were collected using the Mythen microstrip detector[6] from 1.5 to 75° in 2θ. To cover the gaps between detector modules, two data sets, each of 30 seconds in duration, were collected with the detector set 1.5° apart and these were then merged to give a single data set. A slit size of 2 mm was used, to ensure that the fraction of the capillary illuminated by the X-ray beam is the same as the isothermal zone on the cryostream. The obtained raw data were merged using in-house software PDViPER and further process with the Surfer software package. Le-Bail analysis and peak fitting were performed using TOPAS 5 software package.[7]

Magnetic susceptibility. Data were collected using a Quantum Design VersaLab magnetometer equipped with a vibrating sample mount (VSM, 0.3 T, settle mode). Care was taken during this measurement to avoid any solvent loss by loading the sample into a custom-made polyethylene sample tube with a small amount of mother-liquor. The sample holder was fused shut so that solvent loss could not occur during the measurement. Measurements were taken continuously with a range of scan rates (4, 2, 1, 0.5 Kmin^{-1}; Figure S2) over the temperature range 250 - 100 - 250 K. An additional measurement was taken using a PPMS magnetometer (VSM, 0.3 T) over the range 300 – 10 – 300 K (scan rate: 2 Kmin^{-1}; Figure S3).

Thermogravimetric analysis. Data (Figure S1) were collected using a TA Instruments Discovery Thermogravimetric Analyser. The sample was loaded into a platinum sample holder. Data were then collected with continuous ramping at a rate of 1 °C min^{-1} from RT to 500 °C. The sample was held under a continuous flow of N_2 at 10 mL min^{-1} over the entire experiment.

Mössbauer Spectrocopy. ^{57}Fe Mössbauer spectra were recorded with a ^{57}Co source in a Rh matrix on a SEE Co. (Science Engineering & Education Co., MN) spectrometer equipped with a closed-cycle refrigerator system. Data were collected in constant acceleration mode in transmission geometry. Isomer shifts are given relative to metallic iron foil at room temperature. Analysis of spectra were conducted using the WMOSS program (SEE Co, formerly WEB Research Co. Edina, MN). Due to strong absorptions from Pt, relatively low amounts of sample needed to be used to ensure any signal was observed. Care was taken to ensure the sample remained solvated throughout the measurements by placing a small amount of mother liquor with the sample and fusing the sample holder shut.

DFT Computational Calculations. The DFT+U structural optimizations and energy calculations were performed for infinite crystals using the Vienna ab initio simulation package (VASP).[8-11] We used the generalized gradient approximation in the form of the Perdew-Burke-Ernzerhof functional (GGA-PBE) and an effective Hubbard U, in the Dudarev method,[12] of 1.6 eV (which has been shown to provide accurate results for spin-crossover materials in the solid state[13]). The cut-off energy of the plane-wave expansion

was set to 520 eV and the convergence criterion for energy was 10^{-6} eV. The Brillouin zone was sampled at the Γ-point. Structures were optimized with full-unit-cell (incl. volume) relaxtion. The experimental crystal structures were used as starting points.

2.   Materials and synthesis

All chemical agents were purchased from Sigma-Aldrich and used without further purification. All solvents were of reagent grade or higher and used without further purification.

Synthesis of pyridyl ligand

4,2':6',4''-Terpyridine (TPy) was synthesised according to literature.[14]

Synthesis of [Fe$_3$(Pt(CN)$_4$)$_3$(TPy)$_2$(H$_2$O)$_2$]·2EtOH (1).

[Fe$_3$(Pt(CN)$_4$)$_3$(TPy)$_2$(H$_2$O)$_2$]·2EtOH was synthesised by a vial-in-vial slow diffusion techniques. At the base of the larger vial TPy (14.1 mg, 0.059 mol and K$_2$Pt(CN)$_4$ (22.2 mg, 0.059 mmol) were placed. A the base of the smaller vial Fe(ClO$_4$)$_2$·6H$_2$O (15.0 mg, 0.059 mmol) was placed. The small vial was carefully placed inside the larger one and then both were slowly filled with solvent (ethanol: H$_2$O, 1:1, *v/v*). Over a period of four weeks yellow plate-like crystals formed (yield: ~48%). Anal. calcd (%) for C$_{23}$H$_{19}$Fe$_2$N$_9$O$_2$Pt$_2$, C, 28.92; H,2.00; N, 13.2. Found: C, 28.93; H, 1.806; N, 13.27. IR (cm^{-1}): 3317 (w),2977 (s), 2163 (s), 1654 (m), 1448 (m), 1285 (m), 1087 (s), 1045 (s), 875 (s) 925 (s), 797 (s), 729 (m), 613 (m), 443 (m).

Thermogravimetric analysis
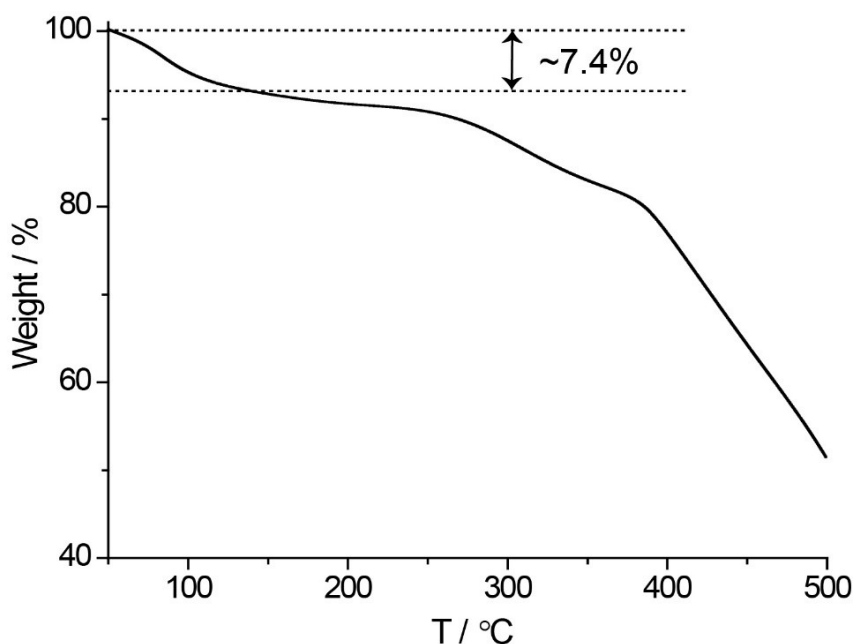
Figure S1. Thermogravimetric analysis data. Between RT and ca. 150 °C there is a mass loss of ~7.4%, this occurs over two steps with the first step (5.2 %; RT - 100 °C) corresponding to ethanol evolution and the second step (2.2%; 100 – 150 °C) accounting for bound water molecule removal.
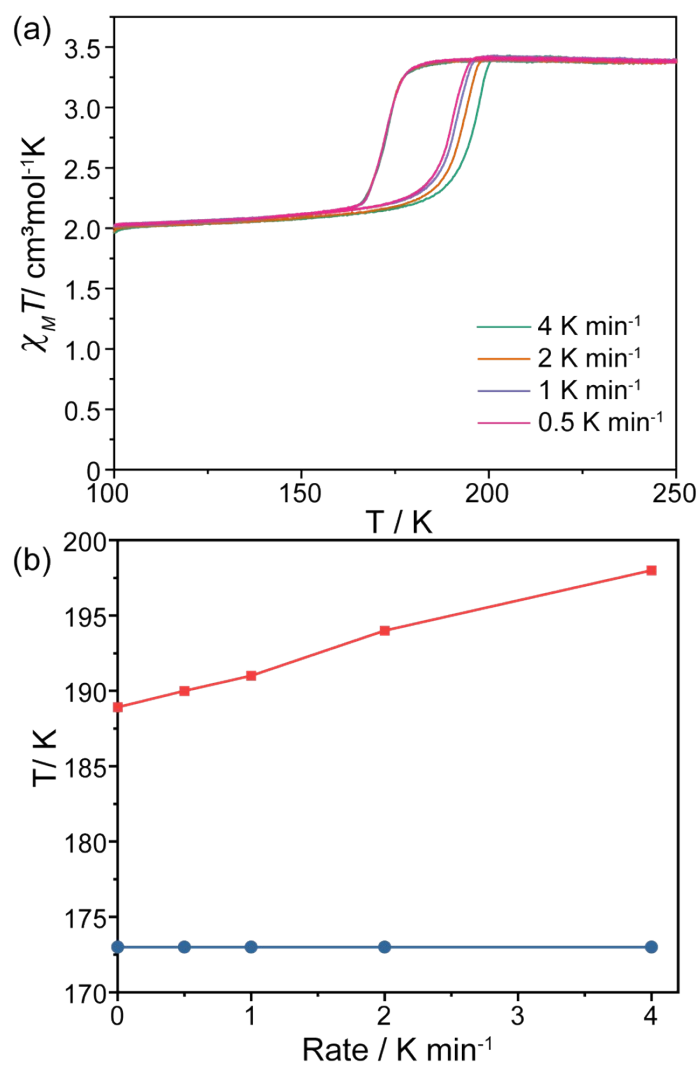
Figure S2: (a) Variable scan rate (4, 2, 1, 0.5 Kmin^{-1}) magnetic susceptibility data (250 – 100 – 250 K) and plot of the transition temperatures versus scan rate. There is some scan rate dependence on the heating curve but not the cooling curve which is relatively common due to kinetic effects.[15]
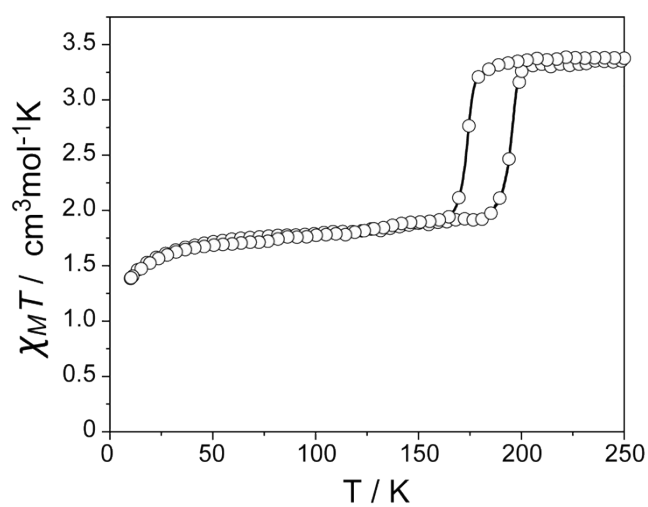

Figure S3. Magnetic susceptibility data over the extended temperature range 250 – 10 – 250 K, showing a small decrease in $\chi_M T$ values below 30 K due to a combination of ZFS and weak antiferromagnetic effects from the remaining HS Fe^{II} ions at this temperature range.
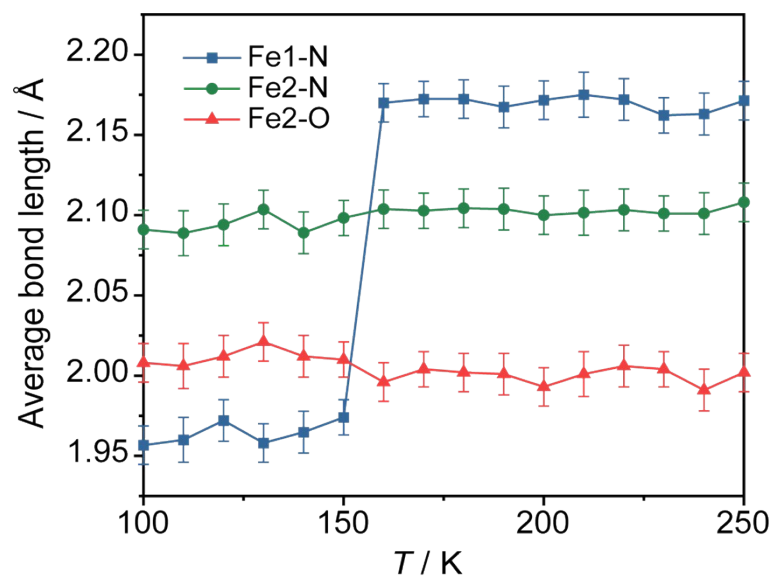
3. Variable temperature single crystal X-ray diffraction
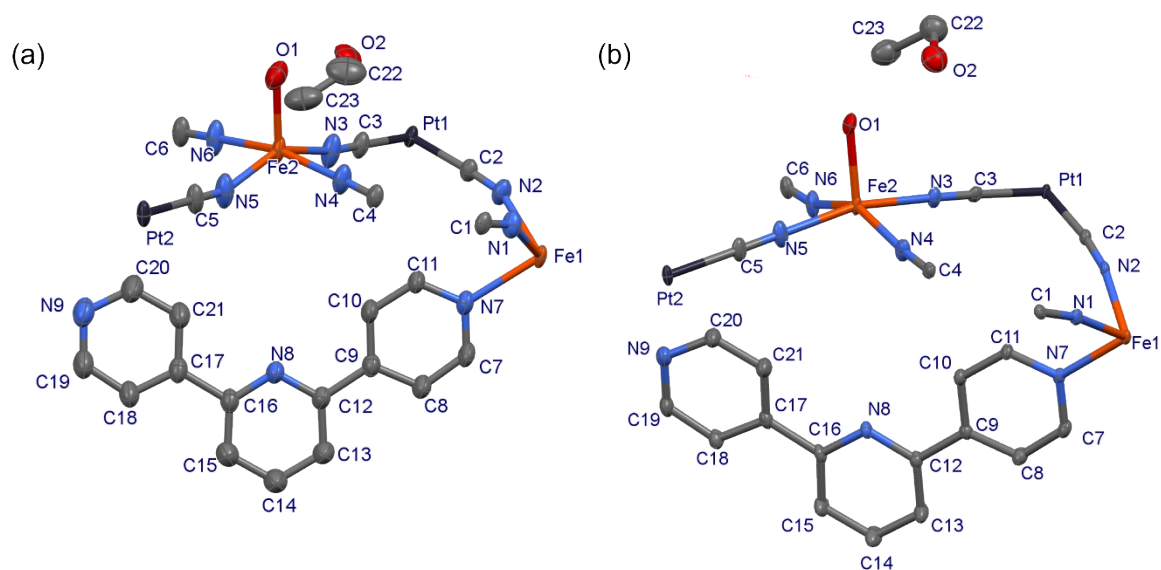
Figure S4. Thermal ellipsoid plot (50% probability) of the asymmetric unit at 250 K (a) and 100 K (b). Hydrogen atoms have been omitted for clarity.
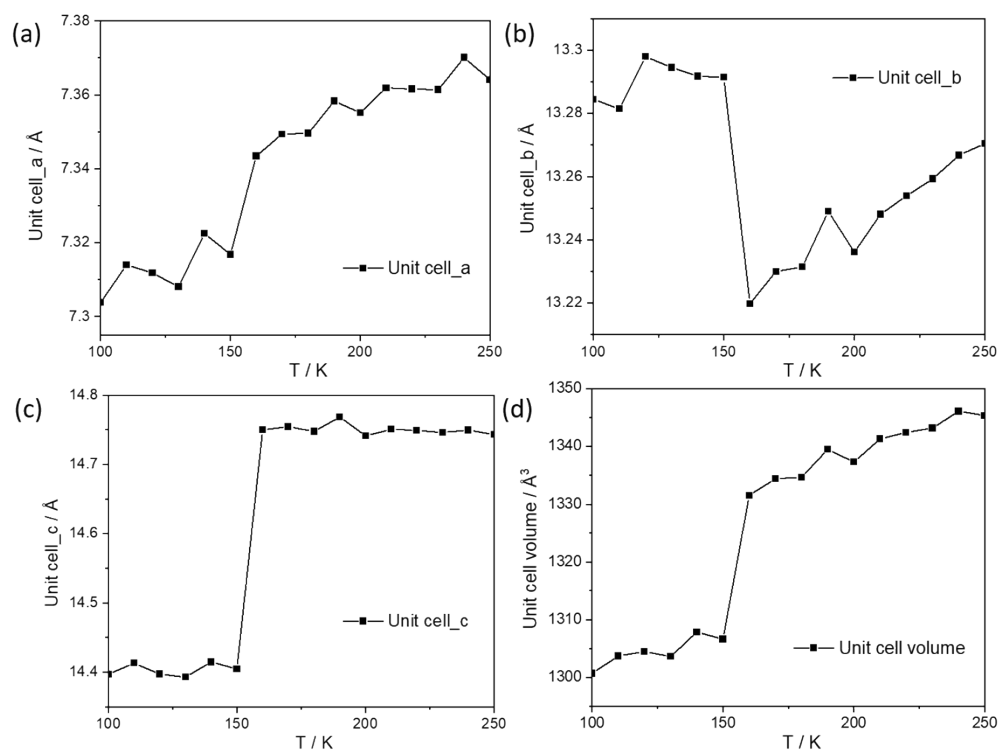
Figure S5. (a) a-axis, (b) b-axis, (c) c-axis and (d) unit cell volume evolution versus temperature (100 - 250 K) from single crystal data.

Figure S6. Variable temperature average Fe-N and Fe-O bond length (100 - 250 K).

Table S1. Single crystal data and refinement details

Formula/ FW	$C_{46}H_{38}Fe_3N_{18}O_4Pt_3$/ 1659.76	
T / K	250	100
Space group	Triclinic *P-1*	
***a* / Å**	7.398(4)	7.3130(4)
***b* / Å**	13.352(9)	13.2786(8)
***c* / Å**	14.812(7)	14.4060(8)
α / °	96.57(3)	96.397(2)
β / °	102.935(16)	103.288(2)
γ / °	103.22(3)	103.500(2)
Volume / Å³	1366.7(14)	1303.55(13)
ρ_{calc}mg / mm³	2.017	2.114
Data/restraints/parameters	5597/257/348	5405/251/340
Goodness–of–fit on F²	1.052	1.049
Final R indexes [I>=2σ (I)][a], [b]	0.0319,0.0760	0.0300,0.0681
Final R indexes [all data] [a], [b]	0.0393,0.0791	0.0372,0.0713

[a] $R_1 = \Sigma||Fo| - |Fc||/\Sigma|Fo$. [b] $wR_2 = [\Sigma[w(Fo_2 - Fc_2)_2)/\Sigma[w(Fo_2)_2]]_{1/2}$.

Table S2. Hydrogen-bond lengths and distance of π-π stacking of **1**.

T / K	O1(H) ⋯ EtOH /Å	O1(H) ⋯ N(Tpy) /Å	π-π stacking/Å
250	2.732	2.707	3.691
100	2.706	2.686	3.665

Model for structural parameter τ

In 5-coordinated systems, there are two possible geometric configurations, square pyramidyl and trigonal bipyramidyl (Figure S6a-b) geometry. In order to better distinguish them, the structural parameter is τ used.[16] The formula of τ is shown in Figure S5d. When the geometry is square pyramidal, the value of τ is 0 and when trigonal bipyramidal τ is 1. The coordination environment of Fe2 is shown in Figure S5c and the calculated τ values (250 K to 100 K) are listed in Table S3. The values are ~0.3 indicating an irregular square pyramidyl geometry.

(a) Square pyramidal geometry
τ = 0

(b) Trigonal bipyramidal geometry
τ = 1

(c)

(d)

$$\tau = \frac{\beta - \alpha}{60}$$

β = ∠N4Fe2N6
α = ∠N3Fe2N5
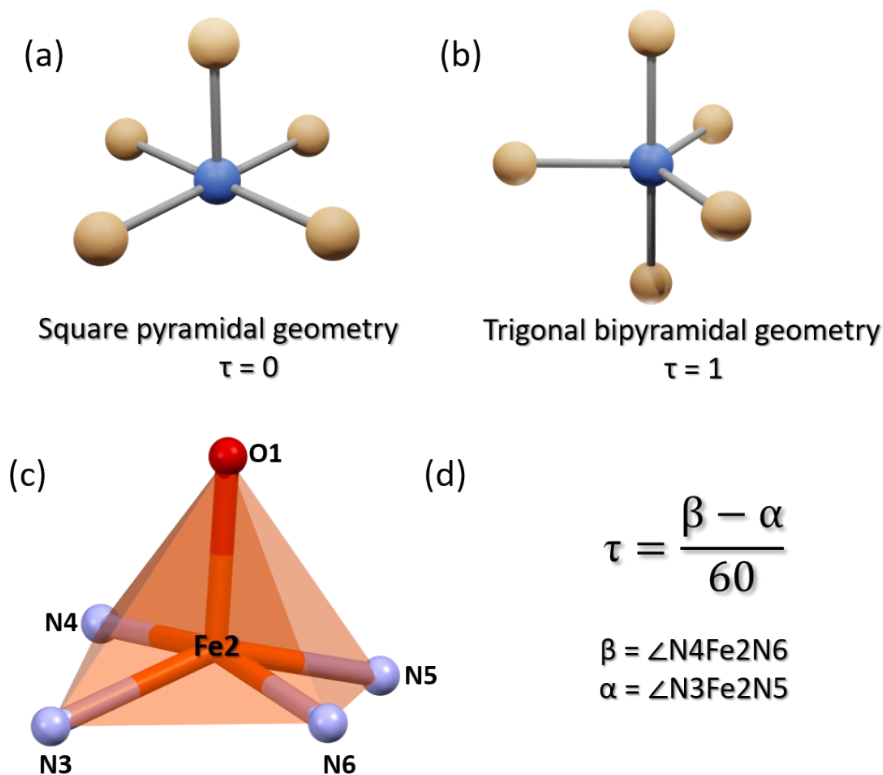
Figure S7. 5-coordinated system geometry for (a) square pyramidal geometry and (b) trigonal bipyramidal geometry; (c) model for 5-coordinated structural parameter τ of Fe2 in **1**; (d) formula for calculation of τ.

Table S3. Temperature-dependence of the distortion angle **Σ** for Fe1 and **τ** for Fe2.

| T /K	d$<_{Fe1-N}>$/Å	d$<_{Fe2-N}>$/Å	d$<_{Fe2-O}>$/Å	ΣFe1 / °	β / °	α / °	τ
100	1.957	2.091	2.008	27.6	167.532	149.148	**0.31**
110	1.960	2.089	2.006	24.4	166.803	150.329	**0.27**
120	1.972	2.094	2.012	22.8	166.307	149.611	**0.28**
130	1.958	2.104	2.021	25.6	166.47	149.306	**0.29**
140	1.965	2.089	2.012	22	166.989	149.095	**0.30**
150	1.974	2.098	2.010	24.4	167.186	149.558	**0.29**
160	2.170	2.104	1.996	15.6	166.708	149.12	**0.29**
170	2.172	2.103	2.004	12.4	167.541	149.641	**0.30**
180	2.172	2.104	2.002	13.2	167.088	149.416	**0.29**
190	2.167	2.104	2.001	16.4	166.676	149.165	**0.29**
200	2.172	2.100	1.993	15.6	166.319	149.57	**0.28**
210	2.175	2.102	2.001	14.4	166.419	149.354	**0.28**
220	2.172	2.103	2.006	15.2	166.482	149.195	**0.29**
230	2.162	2.101	2.004	14.4	166.537	150.687	**0.26**
240	2.163	2.101	1.991	17.1	165.655	150.063	**0.26**
250	2.171	2.108	2.002	14.4	165.777	149.09	**0.28**

Table S4. Summary of Fe-N and Fe-O bond length for reported Fe[II]- and Fe[III]- coordination complexes

Complexes	Spin state	Fe[II]-O	Fe[III]-O	Fe[II]-N	Fe[III]-N
[Fe[II](OEP)(1,2-Me$_2$Im)][17]	HS	-		2.080	
[Fe[II](TpivPP)(NO$_3$)]$^-$[18]	HS	2.069		2.070	
[Fe[II](^{Ph2}Tp)(benzimidazolyl)][19]	HS	1.961		2.139	
[Fe[II](^{Ph2}Tp)(methoxy)][19]	HS	1.931			
[Fe[II](^{Ph2}Tp)(ISQ^{tBu})][20]	HS	2.095		2.099	
K[(N(pi^{Cy})$_3$)Fe[II](OH$_2$)][21]	HS	2.080		2.133	
[(TBimA)Fe[II](benzilate)](ClO$_4$)[22]	HS	2.019		2.161	
$_H$L^{Ph}Fe[II]OH[23]	HS	2.070		2.138	
$_H$L^{cy}Fe[II]OH[24]	HS	2.034		2.162	
$_{Br}$L^{cy}Fe[II]O[23]	HS	2.080		2.143	
[(imSQMe)$_2$FeN$_{240 K}$][25]	HS		1.9153		1.949
[(imSQMe)$_2$FeN$_{100 K}$][25]	LS		1.866		1.897
[Fe[III]−O−MST]$^-$[26]	HS		1. 805		2.021
[1,2-Bis[phenolateiron(III)octaethylporphyrinyl]ethanes][27]	HS		1.916		2.057
[Fe[III](OEP)(2,4,6-trinitrophenol)][27]	HS		1.930		2.049
[Fe[III]OEP) (OPh)][28]	HS		1.848		2.061
diiron(III)-m-hydroxo bisporphyrin[29]	HS		1.925		2.056
MQ-Fe(III)PPIX[30]	HS		1.898		2.065
(2,2'-bidipyrrinato)(μ-oxido)diiron(III)[31]	HS		1.784		2.071
[(PNP)FeCl$_2$][32]	HS				1.981

Precession images

| Temperature / K	0 k l	h 0 l	h k 0
250			
100			
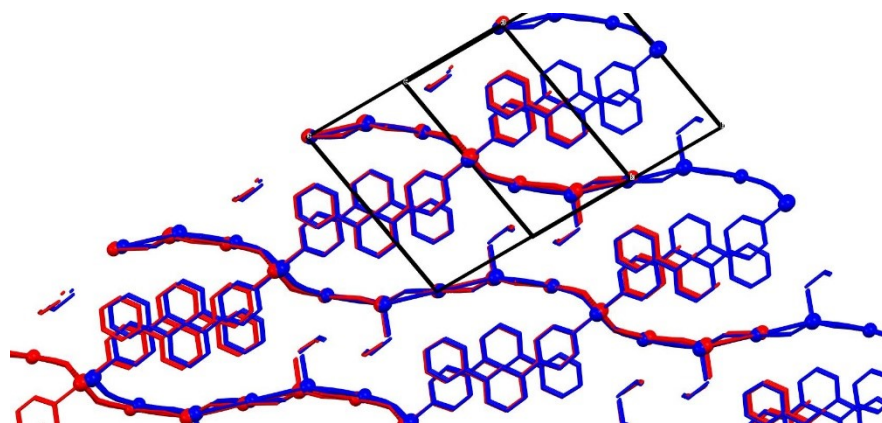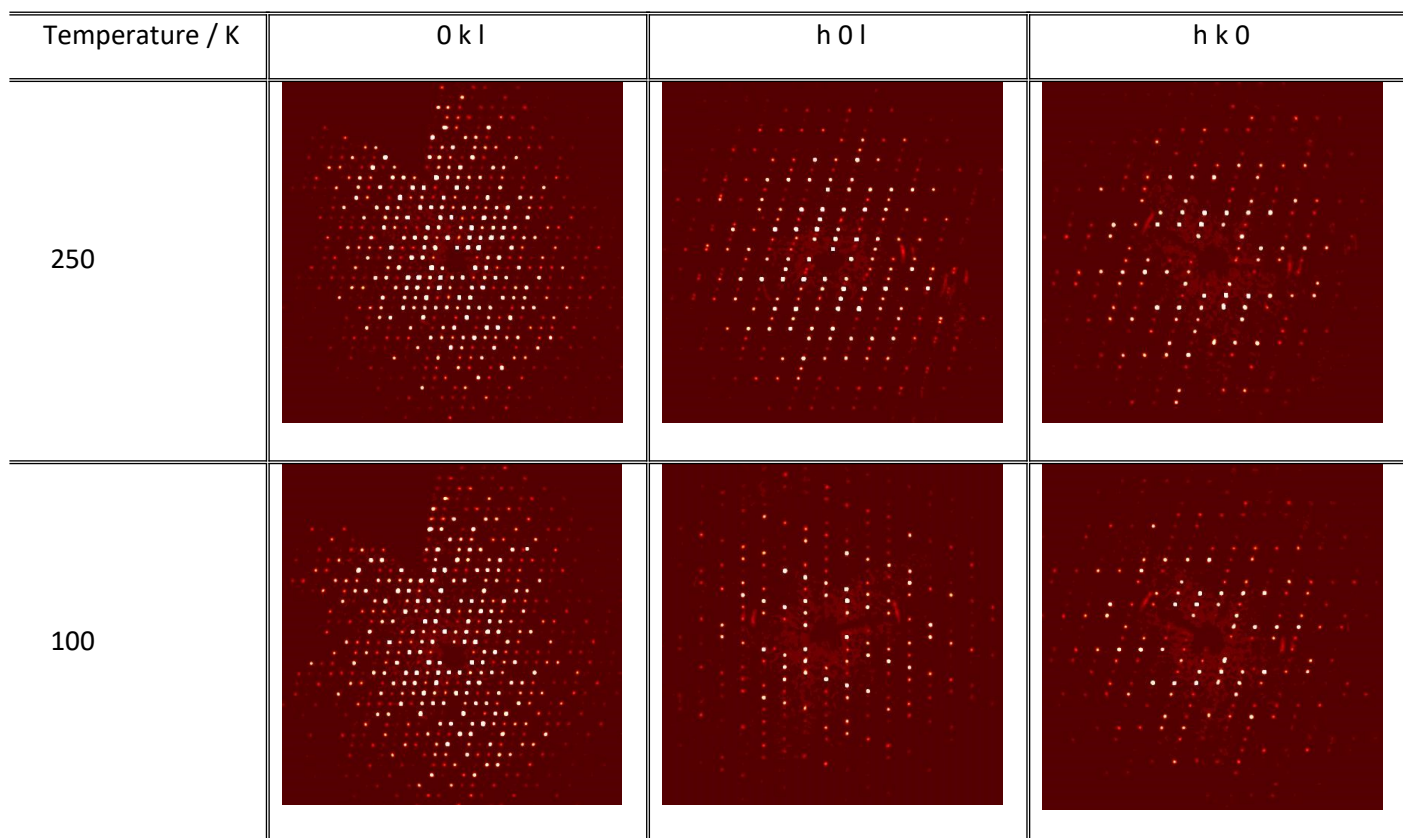
Figure S8. Structural overlay of the 250 K (red) and 100 K (blue) showing the bond length contraction about the Fe1 sites and a small increased deformation of the Hofmann layers (i.e., the mean plane of Hofmann layer passing through Fe1, Pt1 is outside the plane by 1.244 and 1.293 A for 250 and 100 K, respectively, but the Fe2 site does not change. The interlayer spacing decreases from 8.780 to 8.632 Å from 250 to 100 K.
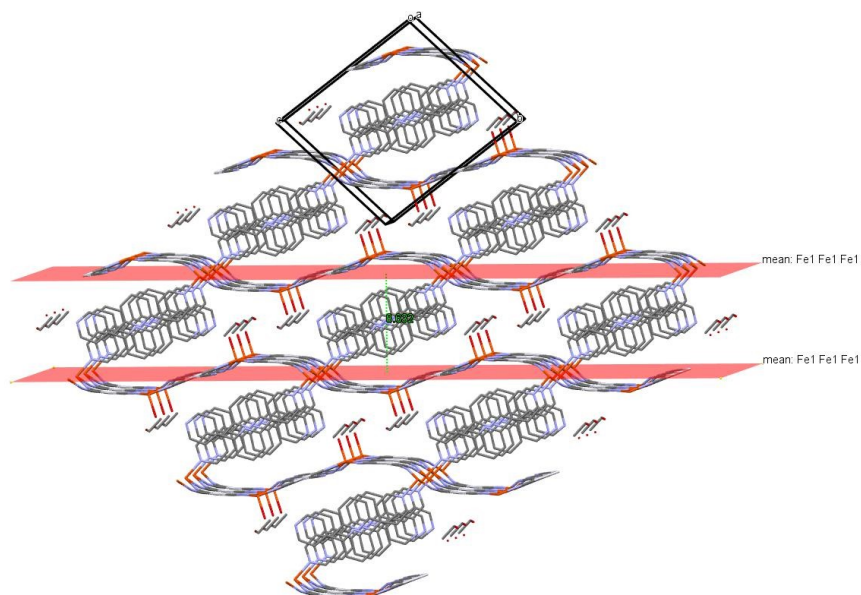
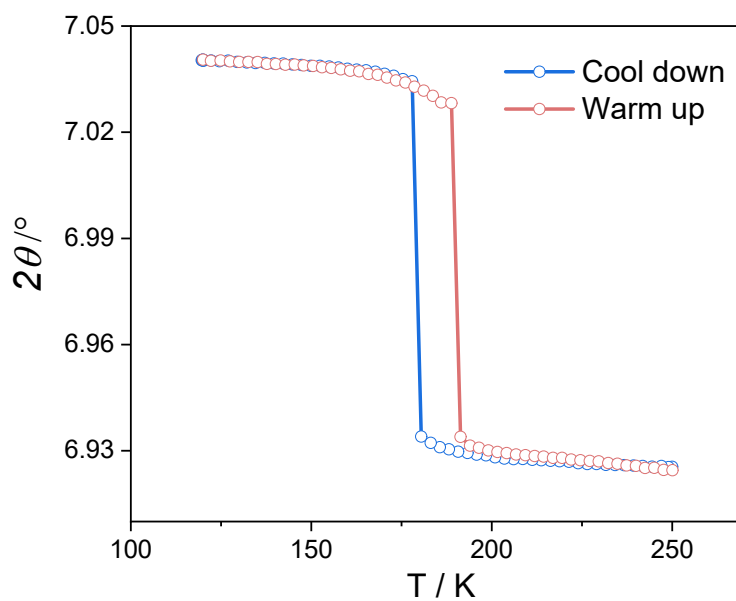**Figure S9** Illustration of the mean plan passing through Fe1 sites.
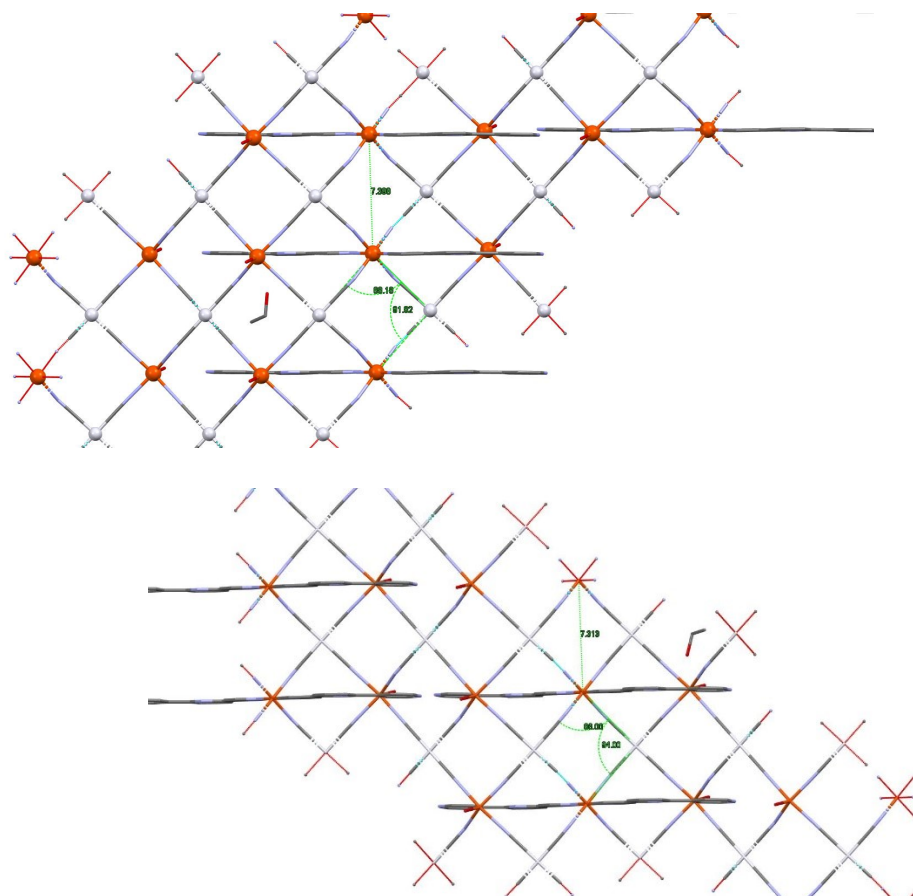
Figure S10. Illustration of the intralayer grid deformation from 250 K (top) to 100 K (bottom). Diagonal Fe1…Fe1 distances 7.398 x 21.046 Å and 7.313 x 20.651 Å for 250 and 100 K, respectively. The square grid angles also show significant change 86 & 94 ° for 250 K and 88.2 & 91.82 for 100 K.

Synchrotron Powder X-ray diffraction
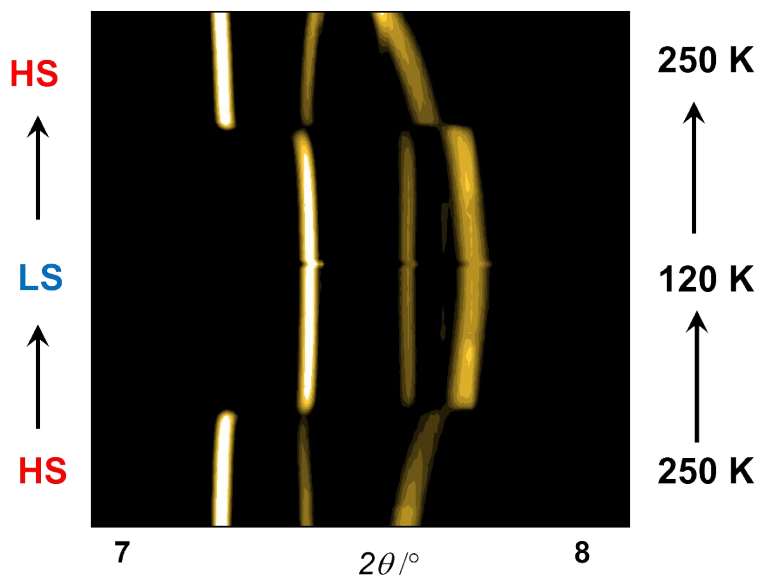
Figure S11. Variable temperature powder X-ray diffraction of **1** showing an abrupt shift in Bragg peaks coincident with the SCO transition from magnetic susceptiblity (temperature range: 250-120-250 K, λ = 0.5895).

Figure S12. Variable temperature powder diffraction peak position evolution of **1**, which shows the transition temperature is consistent to the magnetic susceptibility. (temperature range: 250 – 120 – 250 K, λ = 0.5895 Å).

4. Mössbauer spectroscopy

Table S5. Mössbauer parameters

T / K	Fe1					Fe2				
	δ / mm s^{-1}	ΔE_Q / mm s^{-1}	Γ_L / mm s^{-1}	Γ_R / mm s^{-1}	I / %	δ / mm s^{-1}	ΔE_Q / mm s^{-1}	Γ_L / mm s^{-1}	Γ_R / mm s^{-1}	I / %
294	1.14	1.73	0.39	0.50	46	1.08	0.59	0.25	0.26	54
150	0.46	0.15	0.29	0.29	49	1.23	2.21	0.53	0.60	51
4.6	0.47	0.17	0.26	0.26	43	1.25	2.39	0.75	0.59	57

5. DFT+U results

**Table S6**. DFT+U Optimized structure parameters according to spin state and Fe2 oxidation state. We were unable to converge an Fe^{III} (LS, HS) state despite extensive efforts, which may indicate it is unstable. The **ΣFe1** values were calculated with OctaDist.[33]

Fe2 Oxidation State	Spin state (Fe1, Fe2)	ΔE / kJmol⁻¹	Fe1-N / Å	Fe2-N / Å	Fe2-O / Å	ΣFe1 / °	τ	Vol. / Å³
Fe^{II}	LS, LS	81.9	1.98	1.95	1.99	36.5	0.01	1295
	LS, HS	0	1.94	2.07	2.03	25.8	0.26	1341
	HS, LS	109.2	2.11	1.98	2.03	32.3	0.10	1295
	HS, HS	3.1	2.14	2.07	1.99	14.7	0.34	1384
Fe^{III}	LS, LS	157.7	1.98	1.96	2.05	34.7	0.05	1286
	LS, HS							
	HS, LS	222.0	2.17	1.97	2.03	20.8	0.16	1341
	HS, HS	167.4	2.17	1.96	2.03	20.6	0.16	1382
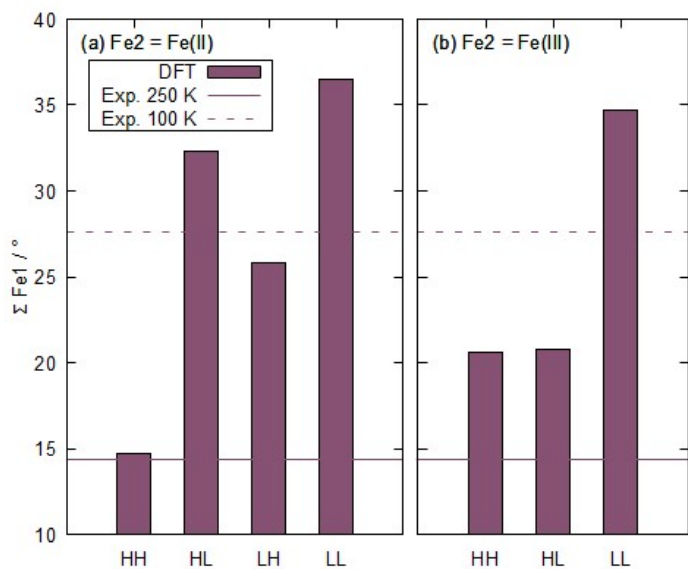
Figure S13. DFT+U ΣFe1 values of **1** (bars, cf. Table S5), compared with those of the experimental structures (lines, cf. Table S3), according to spin state and Fe2 oxidation state. LH = Fe1 LS, Fe2 HS etc.
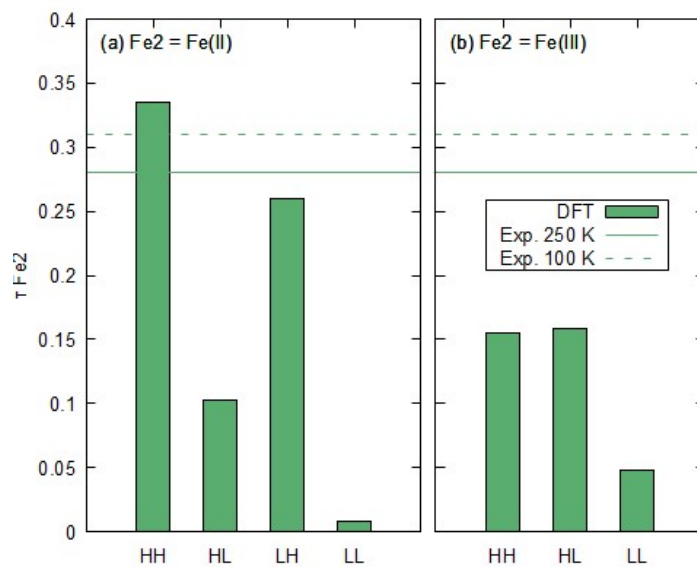
Figure S14. DFT+U τ values of **1** (bars, cf. Table S5), compared with those of the experimental structures (lines, cf. Table S3), according to spin state and Fe2 oxidation state. LH = Fe1 LS, Fe2 HS etc.

References

1. *APEX3*, Bruker AXS Inc.: Madison, WI, 2016.

2. *CrysAlis^{PRO}*, Oxford Diffraction /Agilent Technologies UK Ltd, Yarnton, England

3. O.V. Dolomanov, L. J. Bourhis, R. J. Gildea, J. A. K. Howard & H.Puschmann*, J. Appl. Cryst.*, 2009, **42**, 339.

4. G.M. Sheldrick, *Acta Cryst.*, 2015, **A71**, 3.

5. K. S. Wallwork, B. J. Kennedy and D. Wang, *AIP Conf. Proc.,* 2007, 879.

6. B. Schmitt, C. Brönnimann, E. Eikenberry, F. Gozzo, C. Hörmann, R. Horisberger and B. Patterson, *Nucl. Instrum. Methods Phys. Res., Sect. A*, 2003, **501**, 267.

7. G. Kresse and J. Furthmüller, *Comput. Mater. Sci.*, 1996, **6**, 15.

8. G. Kresse and J. Furthmüller, *Comput. Mater. Sci.*, 1996, **6**, 15.

9. G. Kresse and J. Furthmüller, *Phys. Rev. B*, 1996, **54**, 11169.

10. G. Kresse and J. Hafner, *Phys. Rev. B*, 1993, **48**, 13115.

11. G. Kresse and J. Hafner, *Phys. Rev. B*, 1994, **49**, 14251.

12. S. L. Dudarev, G. A. Botton, S. V. Savrasov, C. J. Humphreys and A. P. Sutton, *Phys. Rev. B*, 1998, **57**, 1505.

13. M. Ohlrich and B. J. Powell, *J. Chem. Phys.*, 2020, **153**, 104107.

14. J. Kim, O. K. Kwak, J. K. Park, K. S. Min and Y. Yoon, *J. Incl. Phenom. Marcrocycl. Chem*, 2014, **79**, 495.

15. R. Kulmaczewski, J. Olguín, J. A. Kitchen, H. L. C. Feltham, G. N. L. Jameson, J. L. Tallon and S. Brooker, *J. Am. Chem. Soc.*, 2014, **136**, 878-881.

16. A. W. Addison, T. N. Rao, *J. Chem. Soc. Dalton Trans.*, 1984, 1349-1356.

17. J. A. Chuanjiang Hu, Bruce C. Noll, Charles E. Schulz, and W. Robert Scheidt, *Inorg. Chem.*, 2006, **45**, 4177-4185.

18. H. Nasri, M. K. Ellison, B. Shaevitz, G. P. Gupta and W. R. Scheidt, *Inorg. Chem.*, 2006, **45**, 5284-5290.

19. A. E. Baum, H. Park, D. Wang, S. V. Lindeman and A. T. Fiedler, *Dalton Trans.*, 2012, **41**, 12244.

20. M. M. Bittner, S. V. Lindeman and A. T. Fiedler, *J. Am. Chem. Soc.*, 2012, **134**, 5460-5463.

21. E. M. Matson, J. A. Bertke and A. R. Fout, *Inorg. Chem.*, 2014, **53**, 4450-4458.

22. B. Chakraborty, R. D. Jana, R. Singh, S. Paria and T. K. Paine, *Inorg. Chem.*, 2017, **56**, 359-371.

23. Z. Gordon, M. J. Drummond, E. M. Matson, J. A. Bogart, E. J. Schelter, R. L. Lord and A. R. Fout, *Inorg. Chem.*, 2017, **56**, 4852-4863.

24. E. M. Matson, J. A. Bertke and A. R. Fout, *Inorg. Chem.*, 2014, **53**, 4450-4458.

25. V. G. Vlasenko, A. A. Guda, A. G. Starikov, M. G. Chegerev, A. V. Piskunov, I. V. Ershova, A. L. Trigub, A. A. Tereshchenko, Y. V. Rusalev, S. P. Kubrin and A. V. Soldatov, *Eur. J. Inorg. Chem.*, 2021, 756-762.

26. S. A. Cook, J. W. Ziller and A. S. Borovik, *Inorg. Chem.*, 2014, **53**, 11029-11035.

27. S. Bhowmik, S. Dey, D. Sahoo and S. P. Rath, *Chemistry - A European Journal*, 2013, **19**, 13732-13744.

28. D. Kanamori, Y. Yamada, A. Onoda, T.-A. Okamura, S. Adachi, H. Yamamoto and N. Ueyama, *Inorganica Chim. Acta*, 2005, **358**, 331-338.

29. S. K. Ghosh, S. Bhowmik, D. Sil and S. P. Rath, *Chemistry - A European Journal*, 2013, **19**, 17846-17859.

30 J. Gildenhuys, C. J. Sammy, R. Müller, V. A. Streltsov, T. Le Roex, D. Kuter and K. A. De Villiers, *Dalton Trans.*, 2015, **44**, 16767-16777.

31. M. Bröring, S. Köhler, T. Ostapowicz, M. Funk and C. Pietzonka, *Eur. J. Inorg. Chem.*, 2009, **2009**, 3628-3635.

32. S. Mossin, B. L. Tran, D. Adhikari, M. Pink, F. W. Heinemann, J. Sutter, R. K. Szilagyi, K. Meyer and D. J. Mindiola, *J. Am. Chem. Soc.*, 2012, **134**, 13651-13661.

33. R. Ketkaew, Y. Tantirungrotechai, P. Harding, G. Chastanet, P. Guionneau, M. Marchivie and D. J. Harding, *Dalton Trans.*, 2021, **50**, 1086.